The Electronic Structure and Transmission Characteristics of Disordered AlGaAs Nanowires

Timothy B. Boykin, *Senior Member, IEEE*, Mathieu Luisier, Andreas Schenk, Neerav Kharche, and Gerhard Klimeck, *Senior Member, IEEE*

***Abstract*—Perfect nanowires may be studied from both the bandstructure and transmission perspectives, and relating features in one set of curves to those in another often yields much insight into their behavior. For random-alloy nanowires, however, only transmission characteristics and virtual-crystal approximation (VCA) bands have been available. This is a serious shortcoming since the VCA cannot properly capture disorder at the primitive cell level: those bulk properties which it can satisfactorily reproduce arise from spatially extended states and measurements which average out primitive cell-level fluctuations. Here we address this deficiency by projecting approximate bands out of supercell states for $Al_{0.15}Ga_{0.85}As$ random alloy nanowires. The resulting bands correspond to the transmission characteristics very closely, unlike the VCA bands, which cannot explain important transmission features. Using both bandstructure and transmission results, we are better able to explain the operation of these nanowires.**

***Index Terms*—Nanotechnology, quantum effect semiconductor devices, quantum wires.**

I. Introduction

SEMICONDUCTOR nanostructures have been the subject of increased theoretical interest in recent years. Most often the theoretical approach is of the effective-mass or **k.p**-type due to the computationally challenging nature of nanowire calculations [1]–[5]. Recently, however, more complete, multiband calculations based on methods such as pseudopotentials [6], tight-binding [7]–[10], or the bond-orbital model [11], [12] have appeared. Regardless of the theoretical method employed, two broad classes of calculation are important for nanowires: transport and bandstructure. In the case of nanowires fabricated from ordered materials [9], [10] both types of calculation have been performed.

Alloy nanostructures present special challenges, particularly with respect to interpreting transmission characteristics and the formulation of approximate bandstructures. Because the virtual-crystal approximation (VCA) can accurately reproduce some bulk gaps and masses it is generally used for bandstructure and transport calculations [7], [8], [11], [12]. When evaluating the VCA (in any of its various formulations) for use in nanostructures it must be remembered that under it, all primitive cells are the same, being composed of identical pseudoatoms chosen to mimic bulk behavior. This approach can be satisfactory in bulk, where spatially extended wavefunctions are responsible for properties such as gaps and masses, the measurements of which naturally average out fluctuations at the primitive cell level. Because of the inability of the VCA to capture these fluctuations, some more recent efforts involve random-alloy calculations for nanostructures: bound states of quantum wells [13]–[15] and densities of states for nanowires [16]. None of these efforts, however, addresses either the issue of approximate bandstructure or its relationship to transport characteristics.

Because the details of disorder are known to be important at the nanoscale [17] in this work we address these issues by performing atomistic random-alloy calculations of both the transport characteristics and approximate bandstructures of $Al_{0.15}Ga_{0.85}As$ nanowires. We employ the AlGaAs system because of its attraction from a theoretical point-of-view: nearly identical AlAs and GaAs lattice constants, so that disorder appears as the random cation distribution. (Later work will treat systems such as InGaAs and SiGe in which the atom positions also vary randomly.) To our knowledge this is the first combined bandstructure/transport treatment of an atomically disordered system in the literature and it allows us to relate features in the transport and bandstructure results in greater detail than previously possible. A unified picture of alloy nanowires emerges, in which the nanodevice (transmission) and nanomaterials (bandstructure) viewpoints complement each other and illuminate the physics of these interesting structures.

II. Approach and Results

We carry out atomistic, random-alloy calculations for free-standing $Al_{0.15}Ga_{0.85}As$ nanowires. The supercell calculations are performed using NEMO3D [17]–[19]. In all cases the underlying tight-binding model is the $sp^3d^5s^*$, spin-orbit model [20], with parameters for GaAs and AlAs given in [21]. The wire cross section is square and its axis lies along the [100] direction; the surface atoms in the x-y and x-z planes are passivated [22] by increasing the dangling-bond energy by 30 eV. The wire is specified in terms of zincblende conventional unit cubes (side $a_0 = 0.565$ nm) as $n_x \times n_y \times n_z$, where n_α is the number of cubes in the α-direction. The unit cell for a square cross section wire is therefore a $1 \times n_y \times n_z$ slab consisting of two pairs

Manuscript received March 21, 2006; revised July 11, 2006. This work was supported in part by the Jet Propulsion Laboratory, in part by the California Institute of Technology, in part by the Office of Naval Research, and in part by the National Science Foundation under Grant EEC-0228390. The review of this paper was arranged by Associate Editor R. Lake.

T. B. Boykin is with the Department of Electrical and Computer Engineering, the University of Alabama in Huntsville, Huntsville, AL 35899 USA (e-mail: boykin@ece.uah.edu).

M. Luisier and A. Schenk are with the Integrated Systems Laboratory, ETH Zurich, 8092 Zurich, Switzerland

N. Kharche is with the Network for Computational Nanotechnology, School of Electrical and Computer Engineering, Purdue University, West Lafayette, IN 47907 USA.

G. Klimeck is with the Network for Computational Nanotechnology, School of Electrical and Computer Engineering, Purdue University, West Lafayette, IN 47907 USA and also with the Jet Propulsion Laboratory, California Institute of Technology, Pasadena, CA 91109 USA.

Digital Object Identifier 10.1109/TNANO.2006.886776

1536-125X/$25.00 © 2007 IEEE

of anion-cation planes (four atomic planes). The wires considered here have the dimension $40 \times 6 \times 6$. The method in [21] and [23] is used to extract an approximate bandstructure from supercell eigenstates computed in NEMO3D [17]–[19] where periodic boundary conditions are enforced along the x direction. Transmission and bandstructure calculations for the same device differ only in the boundary conditions applied at the two y-z planes (i.e., along the x direction: periodic for bandstructure, injection/collection for transmission); detailed atom placements in the wire are identical.

In the transport calculations the semi-infinite emitter (collector) region is identical to the first (last) slab of the nanowire, except in the random-alloy nanowire with GaAs reservoirs. Open boundary conditions are obtained by injecting from reservoir bulk states and separating the reflected and transmitted waves. The device is then solved by a hybrid method [24] combining a recursive nonequilibrium Green's function scheme and a wave function calculation.

The approximate bandstructure of a nanowire calculated with the VCA and from a random-alloy supercell is considered first. While in both cases the bands represent those of the best approximate translationally symmetric nanowire with a $1 \times 6 \times 6$ unit cell possible with each respective method, the calculations differ greatly in the method by which the translationally symmetric system is determined. In the VCA calculation, the cations are all fictitious $Al_{0.15}Ga_{0.85}$ pseudoatoms and all on-site and nearest-neighbor parameters are weighted averages of those for AlAs and GaAs. In the random-alloy supercell calcuation, however, the bands are determined by projecting out Bloch states from the supercell eigenstates and computing a probability-weighted average energy [21], [23]. The random-alloy bands therefore incorporate the wire as a whole, including the random cation distribution, and, as shall be seen below, more accurately describe the wire behavior.

Fig. 1 shows the conduction bands of the nanowire. The VCA bandstructure is exact since the VCA treats all cations as $Al_{0.15}Ga_{0.85}$ pseudoatoms. In contrast, the random alloy the bands are approximate and have associated noisy deviations. Both the VCA and random-alloy results have similar shapes and they agree fairly well near $k = \pi/a_0$. Near $k = 0$, however, the random-alloy bands have a much lower conduction-band minimum. This difference is like that seen in bulk alloy calculations, where the resulting random-alloy gap at $\mathbf{k} = \mathbf{0}$ agrees much better with experiment than does that of the VCA (inset Fig. 1) [21], [23]. In the particular nanowire studied here, the much lower conduction-band minimum at $k = 0$ will be seen to profoundly affect the transport properties.

Fig. 2(a) depicts two transmission coefficients for ordered nanowires. The thin solid line corresponds to the VCA bandstructure of Fig. 1, and shows noiseless, step-like turn-ons in transmission for each available band [10]. The turn-on at around 2 eV corresponds to the bands at around 2 eV at $k = 0.95\pi/a_0$. Each band corresponds to two transmission channels for up and down spins. Since the band-edge minimum is at $k = 0.95\pi/a_0$, four channels turn on. At $E \approx 2.005$ eV the bands hit $k = \pi/a_0$ two channels vanish and the transmission shows a dip to a value of 2. Subsequent bands in the energy range $E < 2.15$ eV result in step-like features of transmission coeffiecients. The interpretation of transmission coefficients and bandstructure corresponds to the one of pure materials [10]. Since the

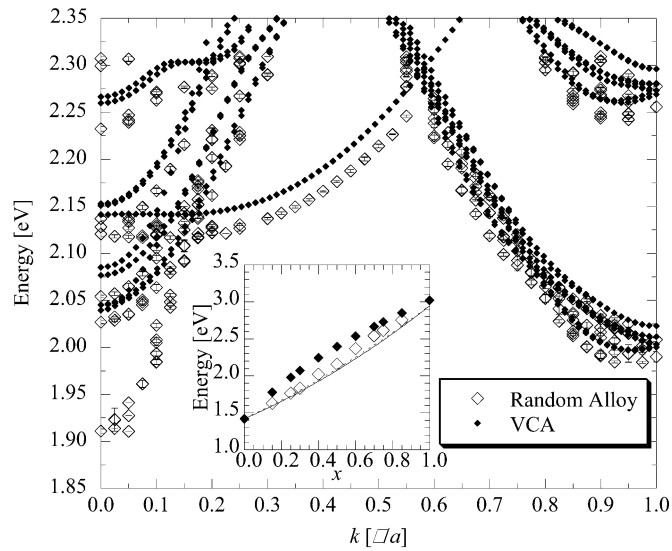

Fig. 1. Conduction bands of the $40 \times 6 \times 6$ $Al_{0.15}Ga_{0.85}As$ nanowire as calculated with the VCA (small solid symbols) and as projected out of random-alloy supercell eigenstates (large, open symbols with error bars). Note in particular that the random-alloy calculation gives a significantly lower minimum at $k = 0$. *Inset:* Gaps of the bulk alloy $Al_xGa_{1-x}As$ at Γ as calculated with the VCA (solid diamonds) and random-alloy supercell projections (open diamonds); lines are experimental results. See [21], [23].

VCA represents pseudoatoms without disorder, this correspondence between exact bandstructure and smooth transmissions is not surprising.

The interpretation of the transmission coefficients in the truly disordered system is, however, more interesting. Fig. 2(b) shows the transmission results for three disordered nanowires. The thick solid line corresponds to the random alloy bandstructure of Fig. 1, which shows its lowest band at $k = 0$ at around 1.92 eV. The transmission coefficient shows a spike at that energy, but not a step-like feature. At about 1.97 eV more channels appear, consistent with the minimum near $k = \pi/a_0$ in the random-alloy bands. Both the local arrangement of atom types and the exact mole fraction (15% Al overall) vary along the wire. The resulting randomness means that the density of states (DOS) is not spatially smooth along the device. Propagating modes therefore differ from slab to slab and one cannot expect the transmission to be a step-like function of energy.

To confirm that these transmission results probe the wire proper and not the reservoirs, we also show the transmission curve for the same random-alloy nanowire, but with GaAs reservoirs (Fig. 2(b), heavy dashed line; spin is neglected for reasons of computational efficiency). Observe that up to about 2.04 eV these results are almost the same as those for the random-alloy nanowire with alloy reservoirs. (For higher energies the spin-orbit interaction becomes more important.) Because similar transmission features are seen in both random-alloy nanowires despite their different reservoirs, we conclude that these noisy features are characteristic of the wire itself.

To demonstrate further that the randomness along the device is responsible for the noisy transmission behavior noted above, we calculate the transmission for an ordered $Al_{0.15}Ga_{0.85}As$ nanowire in which all 40 slabs are identical [light dotted line in Fig. 2(a)]. Here one now sees the smooth transmission

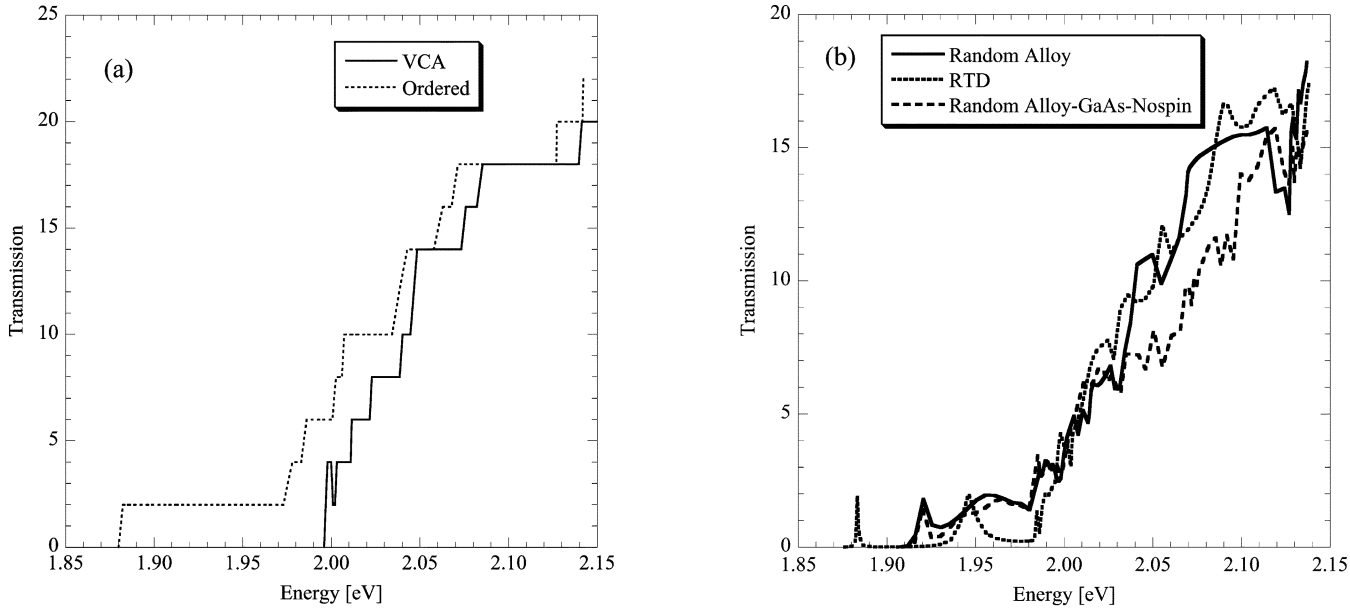

Fig. 2 (a) Transmission characteristics of two $40 \times 6 \times 6$ ordered $Al_{0.15}Ga_{0.85}As$ nanowires. *Light solid line:* VCA nanowire; this nanowire is effectively a pure nanowire made of a pseudomaterial, and shows step-like transmission. *Light dotted line:* nanowire in which all 40 slabs are identical. (b) Transmission characteristics of three $40 \times 6 \times 6$ $Al_{0.15}Ga_{0.85}As$ nanowires. *Dark solid line:* random-alloy supercell wire. *Dark dashed line:* random-alloy supercell wire, but with GaAs reservoirs and neglecting spin. *Dark dotted line:* the special "RTD wire," designed to have an effectively low-gap center. The random-alloy nanowire here is the same (in terms of atom types and positions) as that used for the bands of Fig. 1. Only the boundary conditions (periodic for Fig. 1, injection/collection here) differ.

plateaus found in pure GaAs or Si nanowires [10]. Since both the random-alloy nanowire and the ordered nanowire are nominally composed of $Al_{0.15}Ga_{0.85}As$, they would both be represented by the same VCA nanowire. Note also that the use of a modified VCA (one with an empirical "disorder parameter" to better reproduce the bulk bandgap bowing with composition) [25], [26] would not give correct results, since the noisy behavior in the random-alloy wires is due to the random cation distribution. Although the additional disorder parameter gives better bulk bandgap bowing, the bulk Hamiltonian remains translationally symmetric, so that each small cell (and slab) of the wire would be an identical pseudomaterial. Because both the VCA and modified VCA still represent the alloy as a pseudomaterial, both would treat the ordered and random-alloy nanowires identically. This fact highlights a major shortcoming of the VCA: its inability to truly incorporate randomness, especially disorder at the nanometer scale.

The transmission of the random-alloy nanowire in Fig. 2(b) (thick solid line) shows a peculiar peak at 1.92 eV. Fig. 3 shows the s-anion wavefunction envelopes for the 1.92 eV resonance for the random-alloy nanowire, superimposed over a conduction-band edge profile of the nanowire and the logarithm of the DOS. (For computational efficiency the DOS is calculated neglecting spin since including spin makes little difference for low energy states.) The α-orbital envelope for the slab j is calculated by averaging the square magnitudes of all the α-orbital expansion coefficients in that slab; the conduction band edge profile is calculated assuming each slab were a $1 \times 6 \times 6$ unit cell of a different infinite nanowire. The envelopes and the DOS show a spatially localized, resonance-like feature about the middle of the device at an energy in the middle of (i.e., not above) the conduction band edge fluctuations. The spin-up and spin-down envelopes are concentrated in the lower band-edge regions and are basically symmetric. Each has the characteristic

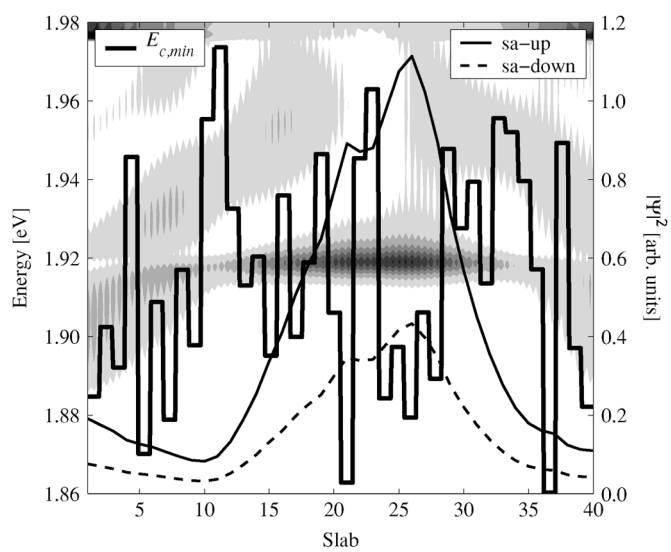

Fig. 3. s-anion envelopes of the spin-up and spin-down orbitals (thin lines) for the random-alloy nanowire superimposed over the wire conduction-band edge profile (thick line) and logarithm of the DOS, neglecting spin (shaded regions). The injected state is spin-up. The emitter reservoir is on the left, hence the slight asymmetry of the envelopes. Note the concentration of the wavefunction in the low-gap region and the similarity in shape to the first resonance of a direct-gap RTD.

of the first quasi-bound state of a direct-gap resonant-tunneling diode (RTD).

To further test this hypothesis, we construct a special nanowire with a quantum well in the center, referred to as the "RTD nanowire" for its resemblance to that device. The wire is made of two different types of $1 \times 6 \times 6$ slabs, both of which have the same cation fractions (15% Al, 85% Ga) but which differ in the distribution of the cations. In the "well" slabs the Al atoms are concentrated near the wire surfaces,

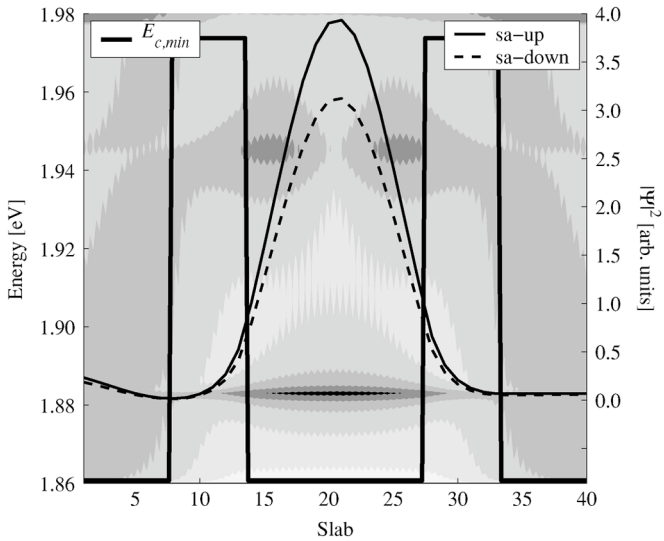

Fig. 4. s-anion envelopes of the spin-up and spin-down orbitals (thin lines) for the RTD nanowire superimposed over the wire conduction-band edge profile (thick line) and logarithm of the DOS, neglecting spin (shaded regions). The injected state is spin-up. The emitter reservoir is on the left, hence the slight asymmetry of the envelopes. Note the characteristic $n = 1$ shape of the wavefunction for the first resonance.

leading to a lower conduction-band minimum, while in the "barrier" slabs the Al atoms are concentrated near the center of the wire, giving a higher conduction-band minimum. The $k = 0$ conduction-band minimum is s-like, with the lowest state symmetric and concentrated near the well center [27]. The transmission characteristic of this wire is shown as the dark dotted line in Fig. 2(b) and its s-anion envelope at the initial resonance (1.88 eV) superimposed over the conduction-band edge profile and the logarithm of the DOS (calculated without spin) is shown in Fig. 4. The second broader resonance at 1.945 eV can be identified in the DOS and the transmission coefficient. Fig. 5 shows the conduction bands of an infinite wire having as a unit cell the "well" slab (solid symbols) along with those of the RTD wire as a whole (open symbols with error bars). Note the similarity of the two bandstructures and the fact that the $k = 0$ minimum of the wire taken as a whole is very much like that of the "well" material.

The s-anion envelopes at the initial resonance are highly symmetric and concentrated in the well, as one expects in an RTD. The bandstructure of the RTD wire further confirms this description. The initial resonant state is composed of counter-propagating Bloch states just above the $k = 0$ conduction-band minimum of the "well" $Al_{0.15}Ga_{0.85}$ As. Injecting carriers into this unbiased structure thus probes the "bulk" (one-dimensional) bands of the quantum well material (here a $1 \times 6 \times 6$ slab) in the same way that injecting carriers into a conventional RTD probes the bulk bands along the growth direction of the quantum well. The RTD nanowire thus behaves in a similar manner to the random-alloy nanowire and its transparent behavior confirms the explanation given for the random-alloy nanowire. The randomness in the alloy wire can therefore lead to localized states that dominate the transport characteristics of the wire. However, these states are formed from the overall wire bandstructure states.

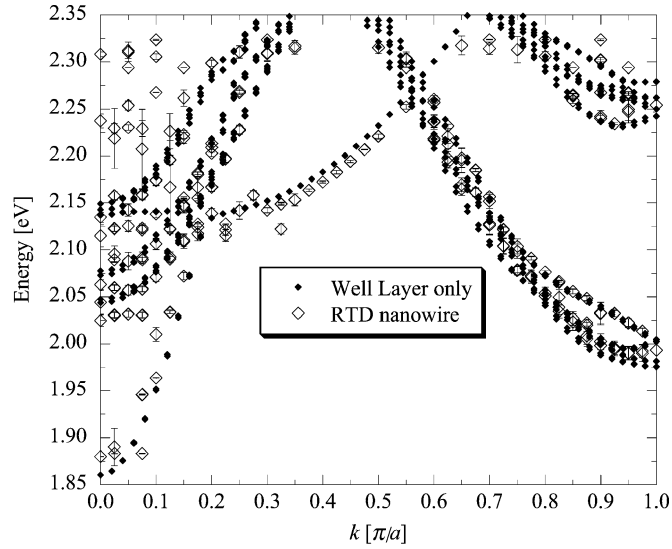

Fig. 5. Bands of the RTD nanowire (large, open symbols with error-bars) and those of an infinite nanowire formed by repeating a single $1 \times 6 \times 6$ slab of the $Al_{0.15}Ga_{0.85}$As from the RTD nanowire well (small, solid symbols). Note the similarity of the two sets of bands.

III. Conclusion

We have seen that the approximate bandstructures of random-alloy nanowires greatly aid in the interpretation of their transmission characteristics, and that the transport results confirm the reliability of and physical meaning attached to, the approximate bands. The availability of approximate random-alloy bands has been seen to be essential for reconciling the transport and bandstructure pictures, since these bands differ considerably from those calculated with the VCA. Because the VCA represents all primitive cells by the same pseudomaterial, its treatment of disorder is too crude to properly resolve the approximate bands of the alloy nanowire, as is clear from the much higher $k = 0$ conduction-band minimum in the VCA. Were only the VCA bands available for comparison with the transmission results, the picture would have been very cloudy indeed. The nanomaterials and nanodevice pictures have thus been shown to be complementary and mutually supporting.

References

[1] L. C. Lew Yan Voon, B. Lassen, R. Melnik, and S. Willatzen, "Prediction of barrier localization in modulated nanowires," *J. Appl. Phys.*, vol. 96, no. 8, pp. 4660–4662, 2004.

[2] L. C. Lew Yan Voon and S. Willatzen, "Electron states in modulated nanowires," *J. Appl. Phys.*, vol. 93, no. 12, pp. 9997–10 000, 2003.

[3] S. Jaziri and R. Ferreira, "Excitonic states of weakly confining quantum wires," *J. Appl. Phys.*, vol. 84, no. 2, pp. 893–900, 1998.

[4] M. Tsetseri and G. P. Tribera, "Mobility in V-shaped quantum wires due to interface roughness and alloy scattering," *Phys. Rev. B*, vol. 69, no. 7, 2004, art. 075313.

[5] H. T. Johnson, L. B. Freund, C. D. Akyuz, and A. Zaslavsky, "Finite element analysis of strain effects on electronic and transport properties in quantum dots and wires," *J. Appl. Phys.*, vol. 84, no. 7, pp. 3714–3725, 1998.

[6] A. Francheschetti and A. Zunger, "Quantum-confinement induced Γ-X transition in GaAs quantum films, wires, and dots," *Phys. Rev. B*, vol. 52, no. 20, pp. 14 664–14 670, 1995.

[7] S. Pescetelli, A. Di Carlo, and P. Lugli, "Conduction-band mixing in T- and V-shaped quantum wires," *Phys. Rev. B*, vol. 56, no. 4, pp. R1668–R1671, 1997.

[8] A. Di Carlo, S. Pescetelli, A. Kavokin, M. Vladimirva, and P. Lugli, "Off-resonance $\Gamma - X$ mixing in semiconductor quantum wires," *Phys. Rev. B*, vol. 57, no. 16, pp. 9770–9779, 1998.

[9] M. P. Persson and H. Q. Xu, "Giant polarization anisotropy in optical transitions of free-standing InP nanowires," *Phys. Rev. B*, vol. 70, no. 16, 2004, art. 161310(R).
[10] Y.-J. Ko, M. Shin, S. Lee, and K. W. Park, "Effects of atomistic defects on coherent electron transport in Si nanowires: Full band calculations," *J. Appl. Phys.*, vol. 89, no. 1, pp. 374–379, 2001.
[11] L.-X. Li and Y.-C. Chang, "Band structures and optical properties of $Ga_{1-x}In_xAs$ quantum wires grown by strain-induced lateral ordering," *J. Appl. Phys.*, vol. 84, no. 11, pp. 6162–6169, 1998.
[12] L.-X. Li, S. Sun, and Y.-C. Chang, "Systematic study of $Ga_{1-x}In_xAs$ self-assembled quantum wires with varying interfacial strain relaxation," *J. Appl. Phys.*, vol. 89, no. 4, pp. 2251–2260, 2001.
[13] B. Koiller, A. S. Martins, and H. Chacham, "Optical effects of interdiffusion in GaAs/AlAs heterostructures: Atomic scale calculations," *Appl. Phys. Lett.*, vol. 69, no. 16, pp. 2423–2425, 1996.
[14] T. G. Dagram, R. B. Capaz, and B. Koiller, "Disorder and size effects in the envelope-function approximation," *Phys. Rev. B.*, vol. 56, no. 15, pp. 9625–9629, 1997.
[15] B. Koiller, R. B. Capaz, and H. Chacham, "Segregation, interface morphology, and the optical properties of GaAs/AlAs quantum wells: A theoretical study," *Phys. Rev. B.*, vol. 60, no. 3, pp. 1787–1791, 1999.
[16] Y. Fu, M. Willander, W. Lu, X. Q. Liu, S. C. Shen, C. Jagadish, J. Zhou, and D. J. H. Cockayne, "Strain effect in a GaAs-$In_{0.25}Ga_{0.75}As$-$Al_{0.5}Ga_{0.5}As$ asymmetric quantum wire," *Phys. Rev. B.*, vol. 61, no. 12, pp. 8306–8311, 2000.
[17] G. Klimeck, F. Oyafuso, T. B. Boykin, R. C. Bowen, and P. von Allmen, "Development of a nanoelectronic 3-D (NEMO 3-D) simulator for multimillion atom simulations and its application to alloyed quantum dots," *Comput. Modeling Eng. Sci. (CMES)*, vol. 3, no. 5, pp. 601–642, 2002.
[18] R. C. Bowen, G. R. Klimeck, W. R. Frensley, and T. Moise, "Quantitative simulation of a resonant tunneling diode," *J. Appl. Phys.*, vol. 81, no. 7, pp. 3207–3213, 1997.
[19] G. Klimeck, R. K. Lake, R. C. Bowen, W. R. Frensley, and T. Moise, "Quantum device simulation with a generalized tunneling formula," *Appl. Phys. Lett.*, vol. 67, no. 17, pp. 2539–2541, 1995.
[20] J.-M. Jancu, R. Scholz, F. Beltram, and F. Bassani, "Empirical $sp^3d^5s^*$ tight-binding calculation for cubic semiconductors: General method and material parameters," *Phys. Rev. B*, vol. 57, no. 11, pp. 6493–6507, 1998.
[21] T. B. Boykin, N. Kharche, G. Klimeck, and M. Korkusinski, "Approximate bandstructures of semiconductor alloys from tight-binding supercell calculations," *J. Phys. Condens. Matter*, to be published.
[22] S. Lee, F. Oyafuso, P. von Allmen, and G. Klimeck, "Boundary conditions for the electronic structure of finite-extent embedded semiconductor nanostructures," *Phys. Rev. B*, vol. 69, no. 4, 2004, art. 045316.
[23] T. B. Boykin and G. Klimeck, "Practical application of zone-folding concepts in tight-binding calculations," *Phys. Rev. B*, vol. 70, no. 11, 2005, art. 115215.
[24] M. Luisier, A. Schenk, W. Fichtner, and G. Klimeck, "Atomisitc simulation of nanowires in the $sp^3d^5s^*$ tight-binding formalism: From boundary conditions to strain calculations," *Phys. Rev. B*, vol. 74, 2006, art. 205323.
[25] S. J. Lee, H. S. Chung, K. Nahm, and C. K. Kim, "Band structure of ternary-compound semiconductors using a modified tight-binding method," *Phys. Rev. B*, vol. 42, no. 2, pp. 1452–1454, 1990.
[26] M. Ferhat, B. Bouhafs, A. Zaoui, M. Certier, B. Kehlifa, and H. Aourag, "Electronic structure of $Al_xGa_{1-x}As$ and GaP_xAs_{1-x} alloys: Modified virtual crystal approximation calculation using sp^3s^* band structures," *Mater. Sci. Eng.*, vol. B41, pp. 304–309, 1996.
[27] M. Luisier, unpublished.

Timothy B. Boykin (S'86–M'91–SM'05) received the B.S. degree in electrical engineering, *summa cum laude*, from Rice University, Houston, TX, in 1987 and the M.S. and Ph.D. degrees in electrical engineering from Stanford University, Stanford, CA, in 1988 and 1992, respectively.

He joined the Department of Electrical and Computer Engineering (ECE) of the University of Alabama in Huntsville (UAH) in September 1992, was promoted to Associate Professor in August 1997, and awarded tenure in August 1998. His research centers on detailed semiconductor heterostructure and device modeling. Highlights of his research include: the first numerically stable localized-orbital basis heterostructure model; the impact of nonzero in-plane wavevector on tunneling; incompleteness in tight-binding models; improved methods for calculating boundary conditions in tight-binding models; optimizations and capabilities of tight-binding models; consequences of incompleteness for the quantum-mechanical continuity equation; the representation of electromagnetic effects in tight-binding models; valley splitting in silicon quantum wells; and modeling alloy nanostructures.

Dr. Boykin won the UAH Foundation Award for Research and Creative Achievement in Applied Science/Technology in 2001. He is a member of Phi Beta Kappa, Tau Beta Pi, Eta Kappa Nu, the American Physical Society, the Institute of Electrical and Electronics Engineers, and Sigma Xi. He has authored or coauthored over 50 refereed journal articles and his first-authored papers alone have been cited by other (noncoauthor) researchers over 300 times.

Mathieu Luisier received the of Dipl.-Ing. degree (with honors) in electrical engineering from ETH Zurich, Switzerland, in 2003. He is currently working toward the Ph.D. degree at the Integrated Systems Laboratory, ETH Zurich, on quantum transport in nanoscale devices (graduation expected in 2006).

From July to December 2005, he was a Visitor at the Network for Computational Nanotechnology, Purdue University, West Lafayette, IN.

Andreas Schenk received the Dipl. Phys. and Ph.D. degrees from Humboldt University in Berlin (HUB), Germany, in 1981 and 1987, respectively.

From 1987 till 1991 he was working on various aspects of the physics and simulation of optoelectronic devices. In 1991 he joined the Integrated Systems Laboratory (ISL) of ETH Zurich, Zurich, Switzerland, as a Senior Research/Teaching Assistant, where he qualified to give lectures at university in 1997 for Physics and Modeling of Microelectronic Devices. In 2004 he became Titular Professor at the ISL. He heads the device physics group at ISL. He authored and coauthored two books and 110 papers. His main activities are in the physics-based modeling for advanced simulation of submicrometer silicon devices and their application in TCAD software. This includes many-body effects, generation-recombination, mobility, contacts, heterojunctions, noise, single-electron transistor modeling at device level, and quantum effects in silicon ultra-small devices with emphasis on barrier tunneling, resonant tunneling, scattering rates, and currents.

Neerav Kharche received the B.Tech. and the M.Tech. degrees in metallurgical engineering and materials science from the Indian Institute of Technology, Bombay, India, in 2003. He is currently working toward the Ph.D. degree in electrical and computer engineering at Purdue University, West Lafayette, IN.

His research interests lie in the area of electronic structure and quantum transport in nanoscale devices. He is currently working on modeling the effects of disorder on the electronic structure of nanowires and quantum wells.

Gerhard Klimeck (S'94–M'96–SM'04) received the German electrical engineering degree from Ruhr-University Bochum in 1990 and the Ph.D. degree from Purdue University, West Lafayette, IN, in 1994.

Previously he was a member of technical staff at the Central Research Lab of Texas Instruments. He was the Technical Group Supervisor for the Applied Cluster Computing Technologies Group and continues to hold his appointment as a Principal Member at the Jet Propulsion Laboratory on a faculty part-time basis. He is the Technical Director of the Network for Computational Nanotechnology and Professor of Electrical and Computer Engineering at Purdue University since Dec. 2003. He leads the development and deployment of web-based simulation tools that are hosted on http://nanohub.org, a community Web site that is utilized by over 15 000 users annually. His work is documented in over 140 peer-reviewed publications and over 234 conference presentations. His research interest is in the modeling of nanoelectronic devices, parallel cluster computing, genetic algorithms, and parallel image processing. He has been the lead on the development of NEMO 3-D, a tool that enables the simulation of tens-of-million atom quantum dot systems, and NEMO 1-D, the first nanoelectronic CAD tool.

Dr. Klimeck is a member of APS, HKN, and TBP.